

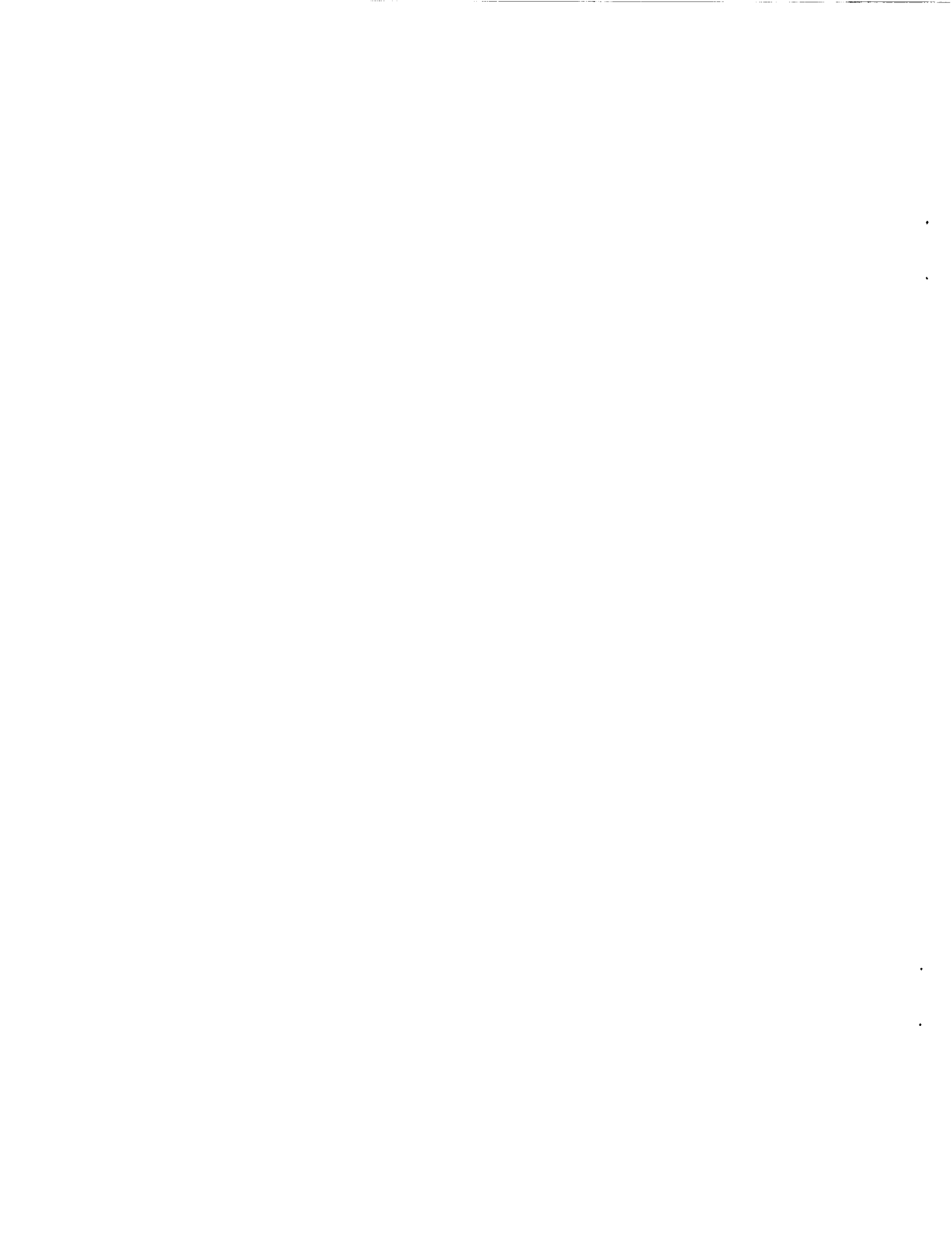


**AIAA 2003-1023**

**Investigation of an Oscillating Surface  
Plasma for Turbulent Drag Reduction**

Stephen P. Wilkinson  
NASA Langley Research Center  
Hampton, VA 23681-2199

**41st Aerospace Sciences Meeting & Exhibit**  
**6-9 January 2003**  
**Reno, Nevada**



Invited Paper**INVESTIGATION OF AN OSCILLATING SURFACE PLASMA FOR  
TURBULENT DRAG REDUCTION**

Stephen P. Wilkinson\*

NASA Langley Research Center, Hampton, VA

**Abstract**

An oscillating, weakly ionized surface plasma has been investigated for use in turbulent boundary layer viscous drag reduction. The study was based on reports showing that mechanical spanwise oscillations of a wall can reduce viscous drag due to a turbulent boundary layer by up to 40%. It was hypothesized that the plasma induced body force in high electric field gradients of a surface plasma along strip electrodes could also be configured to oscillate the flow. Thin dielectric panels with millimeter-scale, flush-mounted, triad electrode arrays with one and two-phase high voltage excitation were tested. Results showed that while a small oscillation could be obtained, the effect was lost at a low frequency (< 100Hz). Furthermore, a mean flow was generated during the oscillation that complicates the effect. Hot-wire and pitot probe diagnostics are presented along with phase-averaged images revealing plasma structure.

**Introduction**

Dielectric-controlled, weakly ionized AC surface plasmas operating at

---

\* Senior Research Engineer , Flow Physics and Control Branch, Senior Member AIAA

"This material is declared a work of the U.S. Government and is not subject to copyright protection in the United States"

atmospheric pressure have recently become a topic of interest for flow control applications<sup>1-6</sup>. The interest stems from the plasma's ability to accelerate ionized air in regions of steep electric field gradients along strip electrode edges. The combination of steep edge gradients and charged particles within the plasma to a body force on the air through an electrodynamic collisional process<sup>7</sup>. The existence of the body force has led to the search for flow control opportunities that can utilize such an effect.

The plasma is typically generated between adjacent, thin, surface, strip electrodes with an intervening dielectric to prevent avalanche breakdown of the air. The most common configuration is thin foil strip electrodes bonded to opposite sides of a thin dielectric panel. The plasma is typically operated in the range of 1-10kHz, 1-10kV rms for the majority of low speed experiments and applications studied thus far. Some of the physical principles on which the plasma and body force generation operate are discussed by Roth<sup>1,2,5,7,8</sup> and Massines<sup>9</sup>. Kunhardt<sup>10</sup> reviews this and similar plasmas and cites additional references.

The present flow control investigation considers the possibility of reducing viscous drag due to boundary layer

turbulence by using a dynamic application of the plasma-induced body forces. The study is based on numerous reports<sup>11-19</sup>, showing that transverse mechanical oscillations of a wall can significantly reduce turbulent drag on that wall by as much as 40% and turbulence intensity by 70%. While these findings are highly significant to understanding the physics of turbulent drag reduction and of boundary layer turbulence in general, the method is not practical for engineering applications due to efficiency and frequency response issues. While the mechanism of drag reduction for the oscillating wall has not been established conclusively, there is clearly an alteration of the quasi-random turbulence production process leading to the observed reduced turbulence intensities and drag. With this background, it was conjectured that oscillating the flow using the plasma-induced body force could also have an impact on the drag. While the details of a impulsive body-forced flow differ significantly from the smooth mechanical wall oscillations, if the basic goal is to disrupt the turbulence, the plasma may be effective as well.

As a starting point, bench studies were initiated on small (<100 cm<sup>2</sup>) plasma panels. A simple interlocking electrode array pattern was selected that enabled the plasma to be oscillated from side to side at variable frequency. The goal was to document the interaction between oscillating plasma and the surrounding air and to use this information to help design a full scale model for wind tunnel testing. Numerous laboratory difficulties related to the models and instrumentation slowed progress and the study at this time is still at the bench testing stage. The main problems

encountered were issues with model robustness, dynamic flow measurement close to or in the plasma, shaping of the excitation voltage to provide the proper body force input and the structure and uniformity of the plasma itself. These issues are discussed along with other relevant material in the following sections. The paper concludes with an assessment of the prospects for success of the control method.

### **Oscillating Plasma Model and Excitation**

A robust plasma model was required that was capable of sustaining the plasma for the long periods required for hot wire or pitot probe surveys. Initial efforts focused on flexible polyimide films (Kapton, Pyralux, etc). Copper electrodes were bonded to the surfaces in a two layer design using conventional electronic flex circuits fabrication methods. While this technology works, it was not optimized for use in this plasma study and frequent burn-throughs of the dielectric between adjacent electrodes at inopportune times during testing led to use of a different design. The initial rigid plasma models<sup>1,2</sup> studied at NASA Langley were very robust and were adopted for these studies. Figure 1 shows the plan views of the models P1 and P2. The electrodes were arranged in triads consisting on one top surface electrode flanked by two bottom surface electrodes. The only difference between P1 and P2 is the number of electrode triads. The upper electrode was 0.1 mm thick pressure-sensitive aluminum tape with an electrically conductive silicone adhesive. The rigid dielectric substrate was 0.75 mm thick type G4 epoxy-woven glass printed circuit board. The models were hand-built with the electrodes registered from top to bottom

visually for a nominal zero electrode overlap as shown. The aluminum tape was bonded to the surface by dragging a smooth, blunt tool along the tape while pressing down along the surface to ensure a secure bond. A 1.2mm thick piece of float glass was bonded to the bottom surface with a slow-cure, low vapor pressure epoxy adhesive designed for use in vacuum systems. The glass provided a smooth mounting surface for the model and suppressed the bottom surface plasma. The bottom electrodes were encapsulated in the epoxy between the G4 dielectric and glass backing plate. Small voids were visible through the glass in the epoxy between adjacent electrodes but no model failures were experienced with this construction technique. Additional pieces of aluminum tape (not shown) were affixed to the numbered edge terminals for attachment of the high voltage excitation clip leads.

The models were typically run at an excitation frequency of 3 kHz. Higher frequencies to more frequent failures. At 6 kHz, models would fail routinely after only short periods of operations. At 10 kHz, only intermittent operations (< 1 minute) could be sustained due to model ignition. Non-plastic dielectrics are more robust but not without problems. One model used thin float glass ( a biological specimen slide) and failed by a microscopic burn-through, presumably at an imperfection site in the glass after sustained use at 3kVrms and 3kHz.

A simplified schematic of the plasma power supply is shown in Figure 2. The input for each channel was provided by a precision, synthesized sine wave generator. The high voltage amplifiers (not shown) were commercial AC

variable frequency power supplies rated at 1kVA each (one per channel). The transformers were custom-built 25:1 turns ratio with a center-tapped secondary. They were rated at 1kVA each. ( The power supplies were rated for larger wind tunnel models, not for the small bench test models shown in Figure 1). Each channel was capable of providing in excess of 10kV rms, more than adequate for the present study run at typically 3 kV rms.

The object was to create a oscillating plasma on the upper surface. In Figure 2, the driving voltages are  $V_1-V_3$  and  $V_2-V_3$ . The trigonometric difference relations for the two voltages assuming for simplicity unity amplitudes are:

$$\begin{aligned} V_1 - V_3 &= \sin(\omega_2 t) - \sin(\omega_1 t) \\ &= 2 \cos\left[\frac{1}{2}(\omega_2 + \omega_1)t\right] \sin\left[\frac{1}{2}(\omega_2 - \omega_1)t\right] \quad 1(a) \end{aligned}$$

$$\begin{aligned} V_1 - V_3 &= \sin(\omega_2 t) - (-\sin(\omega_1 t)) \\ &= 2 \sin\left[\frac{1}{2}(\omega_2 + \omega_1)t\right] \cos\left[\frac{1}{2}(\omega_2 - \omega_1)t\right] \quad 1(b) \end{aligned}$$

Equations 1(a) and 1(b) are the driving voltages for the plasma. Each is seen to consist of a high frequency component (one half of the sum of the input frequencies) modulated by a low frequency component ( one half of the difference of the input frequencies). The two signals are in quadrature or 90 degrees out of phase. This quadrature excitation provides the required input to drive the plasma from side to side on the top surface electrodes in Figure 1. Figure 3 shows actual data for one of the cases tested in this study,  $\omega_1=3000\text{Hz}$  and  $\omega_2=3010$ . It shows the 90 degree phase difference required to produce the oscillatory effect, in this case, at 10 Hz. Since the plasma initiates when the voltage difference between the

electrodes exceeds a particular breakdown level, the plasma forms twice per frequency cycle (i.e. once per single envelope or beat of the modulated waveforms). Reference 20 describes the physics of the initiation and extinguishing of the plasma.

### **Test Apparatus and Diagnostics**

The bench tests were conducted in a clear acrylic plastic enclosure as shown in Figure 4. The box dimensions were 37cm wide by 43cm long by 26cm high. The model was mounted vertically on an acrylic plastic support stand. A three axis (X,Y,Z) commercial stepper-motor probe-survey mechanism was situated outside of the enclosure with the pitot or hot wire probe attached to the end of a non-conducting probe arm. The accuracy of the probe placement including survey mechanism accuracy, alignment and initial position uncertainty is estimated to be 0.1mm or better. An opening in the enclosure allowed for the range of probe motion required for the flow mapping surveys. Safety protocol required that the only conductors crossing the enclosure boundary were the high voltage excitation leads from the power supply. All other objects or signals crossing the boundary were either non-conducting or optically isolated.

A hot wire anemometer and a miniature pitot probe were used to measure the plasma induced flow. The hot wire anemometer was a simple, bread-boarded, uncompensated constant current unit. The choice of this over more capable units was based on fear of damage to the unit while probing in or near the high voltage plasma, a fear that in retrospect turned out to be unfounded. The lack of frequency compensation

limited the scientific output of these experiments but provided adequate information on which to base assessments of the flow control method.

A simplified schematic of the anemometer circuit is shown in Figure 5. The unit was battery operated and totally self-contained. It was situated in the test enclosure along with the hot wire and connecting cable. The anemometer output was optically transmitted to the data acquisition system by a custom-built optical isolator. The isolator consisted of an LED modulated by the anemometer output through transistor Q1, a 150mm non-conducting opaque tube crossing the test enclosure boundary and a optical receiver (phototransistor) at the other end of the tube. The optical isolator had a very linear transfer function but since the anemometer system (probe, electronics, isolator, data acquisitions filter/amplifier) was calibrated as a whole, characteristics of individual items are not called out. For most test cases, the anemometer was electrically isolated (i.e., floating) with respect to the high voltage power supply or the earth ground. This ensured that only the differential anemometer output was recorded regardless of any electromagnetic pickup (common mode voltage) of the anemometer system as a whole. Unsuccessful attempts were made to operate the anemometer in other than a fully isolated condition and are discussed in the *Results - Hot-Wire and Pitot Probe Issues* section.

The hot wire probe consisted of a single 5 micron platinum-plated tungsten wire, approximately 1.5mm long. The anemometer circuit was designed to run the probe at a fixed nominal resistance

or overheat ratio of 1.5. The probe was calibrated in a small, compressed air open jet adjacent to the test enclosure using the same probe cable as for the plasma measurements. The maximum calibration velocity was about 2.5 m/sec. The no-flow output voltage was offset to nominally zero and low pass filtered appropriate to the test (typically 10 Hz for DC measurements and 0.1-3 kHz for dynamic data). Calibration data was fit to a fourth order polynomial for converting raw data to velocity.

The anemometer was not temperature compensated which caused a drift bias error as the probe was moved from the calibration jet to the test enclosure and during the plasma runs. No precise attempt was made to quantify error although observing the no-flow zero shifts suggests that a 15-20% absolute error is likely. For a given run, however, under constant conditions and using the same calibration, the relative magnitudes should be much better. The quantitative anemometer data should, therefore, be used judiciously. Other important hot wire issues such as behavior in or near plasma, frequency compensation, wire orientation, wall proximity effects and use in a still air environment are discussed with presentation of the actual data.

A pitot probe was also used in one set of mean flow measurements. It consisted of a 1 mm OD by 0.1mm wall thickness stainless steel tube. The probe end was flattened to 1.35 mm wide by 0.57mm high. Dynamic pitot pressure was referenced to the atmosphere and measured with a 10mmHg full scale capacitive gage. The pressure accuracy is 0.01%, however, the derived velocity accuracy depends on flow angularity,

wall effects and possible plasma effects making the absolute accuracy difficult to predict. As in the case of the hot wire data, any quantitative data for the pitot tube should be used judiciously.

The plasma was photographed to obtain instantaneous and phase averaged photos of its structure. An intensified charge-coupled-device (ICCD) camera (Cooke Corp. DiCam Pro SVGA) was used with a long distance microscope lens. The camera's image intensifier used a S20 photocathode and a P43 phosphor screen. The ICCD camera was triggered by a delay timer circuit. The circuit received an input pulse from one of the plasma signal generator's sync output and delivered a variable width, variable delay trigger pulse to the camera. The trigger pulse width determined the duration of the exposure. Since the voltage and current in the plasma are approximately 90 degrees out of phase (due to the transformer-coupled power supply), the phase-average was based on the current waveform. Figure 6 shows a typical trigger with respect to the plasma current. In this case, a 10 microsecond ICCD capture occurs at the instantaneous anode and cathode of the plasma. The basic camera output was 1280x1024 pixels which was binned with a 2x2 factor to increase brightness. The combination of short exposure, a dim plasma and the microscopic lens required that binning (accumulation of neighboring pixels into one) be used to obtain a visible image against the background noise even with the image intensifier. The ICCD camera acquisition rate (frame rate) to the computer memory was about 20 frames per second.

The plasma excitation voltage and currents were measured with a 20kV, 75kHz 1000:1 high voltage probe and a 100 kHz bandwidth current monitoring toroidal transformer. Voltages  $V_1$ ,  $V_2$  and  $V_3$  in Figure 2 were measured with the high voltage probes and driving voltage differences  $V_1-V_3$  and  $V_2-V_3$  were formed with two analog op-amp difference circuits. All dynamic data was acquired with a 1Ghz band-width digital oscilloscope. The particular model used had enhanced resolution and peak detection modes that proved very useful in these experiments. The enhanced resolution uses real time averaging to increase voltage resolution and reduce noise. The peak detection mode combines data from several time sweeps to capture short duration voltage spikes that may otherwise not be recorded. This was particularly useful in capturing plasma current waveforms.

## RESULTS

### ICCD images

Figure 6 shows phase-averaged images on the plasma along an electrode edge under steady state excitation. The camera's image acquisition input trigger is shown with respect to the plasma current waveform above each photograph. The shape of the current waveform and the location of the plasma breakdown varies with model size and design (electrical load). The current waveform was acquired in enhanced resolution mode on the oscilloscope which suppresses the high amplitude noise due to the plasma breakdown. The camera is focussed on a plan view of the electrode and the top surface electrode edge is horizontal along the bottom portion of each image. The digital images have been enhanced to

improve display quality. Each image was processed with an un-sharp mask to improve contrast and a median filter to reduce noise. The trigger pulse was 10 microseconds in duration. The CCD sensor in the camera only acquired data while the trigger level was high. These photo's were obtained for one of the flex-circuit Kapton models used early in the study. The electrode is copper in this case. The aluminum tape models showed the same behavior.

The image on the left was taken when the top electrode was the instantaneous anode corresponding the positive current half-cycle and the photo on the right for the negative half-cycle or cathode. Looking ahead at Figure 13(b), the total duration of the plasma for either the anode or cathode is about 150-160  $\mu$ sec out of the total cycle period of 333  $\mu$ sec. For the remaining cycle time, no plasma light is observed. This shows that there are clearly two distinct plasma "pulses" per excitation cycle, one for the instantaneous anode and one for the instantaneous cathode.

There are two primary and significant features evident in the Figure 6 images. First, the plasma distribution along the electrode edge is very non-uniform. This is presumably due to local irregularities or asperities along the electrode's edge. An attempt was made to polish the electrode edge on a different, hand-built aluminum-tape-electrode model. While the uniformity can be increased somewhat, there appear to be limited gains with this approach. The second noteworthy feature is the fundamentally different structure of the anode and cathode images. Whereas the anode image resemble discrete "fountains", the cathode image shows clear structure in

closed loops and bridging across peaks of the plasma structures. In both images, the location of the structures was very repeatable. On an instantaneous basis, within any single 10 microsecond trigger duration, only 1 or 2 flashes of light occur which accumulate with averaging into the images shown. It is clear, therefore, that the plasma is both spatially and temporally non-uniform. The extent to which this non-uniformity affects the induced body force, flow uniformity and device efficiency is not known. Additional ICCD phase averaged images are presented with the pitot probe data regarding plasma formation on the pitot probe itself.

#### **Hot-Wire and Pitot Probe Issues**

Two dimensional hot-wire surveys were conducted for models P1 and P2 with both steady-state and oscillating plasmas. Before presenting this data however, a number of issues with both the hot-wire and pitot tube must first be discussed. First, the plasma tests were conducted in a still air environment within the test enclosure. The absence of an imposed free stream velocity causes interpretation difficulties with both instruments aside from any additional considerations due to the plasma. The electrodes on both models are oriented vertically and the surveys were conducted in the X-Y plane (see Figure 1). The single element hot wire was therefore also oriented vertically. Since there was no free stream flow, the hot wire responds mainly to the magnitude of the local 2D velocity vector,  $(U^2+V^2)^{0.5}$ , and not the flow direction. The pitot tube on the other hand will be in error to the extent that the flow is not aligned with the tube axis. As seen in the PIV measurement

data for a configuration similar to the current models<sup>3</sup>, the angle can be as high as 45 degrees away from the top electrode. If the pitot probe is aligned with the surface, the velocity error can be significant.

The absence of a free stream flow makes the hot wire subject to free convection effects at low velocities. The vertical orientation of the hot wire causes a thermal convection plume to develop enveloping the wire. This plume adds to the usual heat conduction wall interference effect for data obtained very close to the wall. As the probe approaches the wall in still air, the plume around the wire becomes restricted and distorted decreasing cooling of the wire. This leads to an increase in wire temperature and resistance which shows up as a velocity error. Figure 7 shows that the error increases rapidly below about  $Y=0.3\text{mm}$ . This is a worst case since in practice, some velocity exists near the wall which reduces the error. The conclusion is that care must be exercised in interpreting data very close to the wall to see if it can be explained by a wall proximity effect.

Another issue with the hot wire is the use of an uncompensated anemometer. There was no technical reason not to compensate the wire. As mentioned earlier, the issue was one of uncertainty over possible electrical damage to the circuit in the high voltage environment. Using a simple and inexpensive anemometer to start with, confidence was built that with normal care, the anemometer was not in any danger of damage due to any high voltage phenomena. In fact, the anemometer proved to be trouble free after weeks of daily operation which included one

episode in which the probe was inadvertently grounded while approaching a high voltage electrode. The hot wire prongs were instantly destroyed but the directly connected electronic anemometer circuit survived unharmed. The frequency response issue due to the lack of compensation is discussed further with regard to the oscillating plasma results.

In order to obtain either hot wire or pitot data in close proximity to the plasma, the problem of a glow discharge forming on the probe itself was an issue. Since the glow is associated with generation of a body force and acceleration of the air, evidence of glow on the probe indicates probable error in the data. In the case of the pitot probe, the actual dynamic pressure at the probe tip can be reduced by a plasma-induced flow emanating from the probe itself. This was discovered while testing methods to move the pitot probe closer to the top electrode while avoiding a discharge due to high polarization of the metallic probe.

Figure 8 shows phase averaged ICCD images (previously introduced for Figure 6) of the pitot probe close to the upper electrode. Four conditions are shown each with anode and cathode triggering (see discussion of Figure 6). In condition (a), the top electrode is at the excitation voltage, the bottom electrode (on the other side of the model, see Figure 1) is grounded ( $V=0$ ) and the pitot probe is electrically isolated. No glow on the probe is observed. If the probe is moved closer to the electrode, a filamentary discharge (distinctly different from the glow discharge plasma) forms between the probe and the electrode. To eliminate this discharge,

the probe was tied to the excitation voltage in (b). While the filamentary discharge is eliminated (since the electrode and probe are now at the same potential) a glow discharge plasma forms between the probe and the bottom electrode through the dielectric panel. Notice the distinctive anode and cathode structure for each triggering condition. For this condition (b), the measured pitot pressure was approximately zero. The reason is that the pitot probe and top electrode generate flow in opposite directions.

For conditions (c) and (d), the voltage on the top and bottom electrodes were reversed. The condition where the top electrode was at the excitation voltage and the probe grounded or visa-versa was not possible since there would be no intervening dielectric to prevent arcing. The image for condition (d), cathode trigger, is missing but would be similar to (c), cathode trigger, directly above it. The images are reversed from (a) and (b) since the trigger was derived from the signal generator for the top electrode.

#### **Steady-State Plasma – Mean Flow**

Given the issues raised above with respect to hot wire and pitot measurements and the accuracy issue of the hot wire due to temperature drift and also the low speeds, Figure 9 shows a comparison of the two techniques for a steady, plasma-induced mean flow. Note that the that the sizes of the survey regions are different for the hot wire and pitot data. The pitot region is a subset of the hot wire region. The aspect ratio of the contour maps is 1:1.

The plots have some evident differences in the color mappings but largely show the same general structure. The hot wire

measures velocity magnitude from any direction and has a known wall interference effect below about  $Y=0.5$  mm (see Figure 7). The pitot measures stagnation pressure at the tip and will be in error for any flow angularity. The pitot probe tip height is two orders of magnitude greater than the hot wire diameter and averages the pressure over the face of the probe. Given these issues, the peak velocities of 1.6 and 1.3 m/s for the hot wire and pitot respectively appears to be reasonable results. The maps suggest that the maximum velocity lies to the left of the map in the vicinity of the top electrode as would be expected since that is the location of the maximum electric field gradient and body force. Since this region is within the plasma, discharges from metallic probes limits probe measurements in this area.

Figure 10 shows velocity magnitude profiles at seven X locations from the hot-wire map of Figure 9. The curves are spline curve fits to the actual data and pass smoothly through each data point. The data symbols are not shown for clarity. The figure shows decelerating, broadening profiles consistent with a wall jet as expected. Some of the data is below  $Y=0.5$ mm and at the lowest velocities, the wall proximity effect shown in Figure 7 is applicable. Overall however, the data seem to capture the structure of the flow well.

#### **Oscillating Plasma – Mean and Fluctuating Flow**

Models P1 and P2 were run with oscillating plasmas over the range of 5-80 Hz. The upper frequency corresponded to the frequency at which the signal-to-noise ratio for the

anemometer approached unity. Hot wire velocity magnitude data were acquired on two dimensional grids similar to Figure 9. The peak of the excitation amplitudes ( $V_1-V_3$  and  $V_2-V_3$ , see Figures 2 and 3) were set to be the same as for the steady state case. Figure 11 shows the relative rms amplitude of the peak fluctuating velocity near the top electrode on model P1. The peak was obtained from contour maps of the rms amplitude at each test frequency. Tracking the peak rms was chosen over monitoring a fixed spatial location since the rms spatial distribution changed with frequency. From 5 to 80 Hz, the peak rms velocity moved 2.5mm closer to the top electrode. The data in Figure 11 are normalized by the measured peak fluctuation rms amplitude at 10Hz.

Also shown in Figure 11 is the uncompensated thermal response of a 5 micron Platinum-plated Tungsten wire with microwave heating<sup>21</sup>, the same size and type of wire used in the current experiments. The frequency response of the wire varies with stream velocity and the data shown are for the case of zero stream velocity. The figure shows that roll-off in the measured fluctuations exceeds the roll-off in the uncompensated wire response. From 10 to 80 Hz, the model amplitude data (symbols) fall by 15db with less than a third of that attributable to the uncompensated hot-wire. Also, the data roll-off at a rate consistent with that of a first order system or  $-20$ dB/decade as shown by the dashed line. The reason for this response is not known. Discussion of the frequency requirements for oscillating the flow will be discussed in the next section along with the impact of this finding.

Figures 12(a-d) are peak normalized contour plots of the mean and fluctuating velocity magnitudes for model P2 at an oscillation frequency of  $\omega_2 - \omega_1 = 20$  Hz. The vertical coordinate (Y) is stretched by a factor of three to show more detail near the wall. The thickness of the dielectric panel is correct but the height of the electrodes is exaggerated for visibility.

The unexpected feature of Figures 12(a) and (c) is that a mean flow forms in the vicinity of the top electrodes. The reason for this can be found in Figures 13(a) and 13(b). Figure 13(a) shows one of the excitation signals from the power supply (also shown in Figure 3) along with the AC current through the model. The noisy bulges in the current waveform correspond to plasma formation along the electrodes. Figure 13(b) zooms in on a one millisecond segment near the peak of one of the voltage envelopes in Figure 13(a). ("Envelope" refers to the section of increasing/decreasing voltage between zero crossings in Figure 13(a)). As seen in Figure 13(b), the plasma forms twice per excitation cycle, once for the anode and once for the cathode with the cathode plasma being the more energetic of the two. Figure 13(a) shows that plasma duty cycle is about 65% of each envelope or equivalently, the plasma is on 65% of the time on each electrode edge. Recall that there are two excitation signals 90 degrees out of phase (see Figure 3). Since the duty cycle is greater than 50%, the plasmas on each edge of the top electrode overlap in time, in this case by 30%.

The plasma is clearly on for too long and creates the undesirable mean flow. In Figure 13(a), the plasma turns on shortly

after each voltage zero crossing between the envelopes and turns off shortly before each zero crossing. These points correspond to the air breakdown voltage. For a sinusoidal excitation voltage and a fixed breakdown threshold, the duty cycle will vary with the amplitude of the excitation voltage. In the limiting case where the excitation amplitude is equal to the breakdown threshold, the duty cycle is zero. As the excitation amplitude increases, so does the duty cycle. The strength of the plasma and body force depends upon the excitation amplitude. For an amplitude just above the breakdown threshold, the duty cycle will be short but the plasma will be weak. For an excitation amplitude much greater than the breakdown threshold, the plasma will be strong but the duty cycle will be long. Its clear that a sinusoidal envelope is not well suited to this application. A more suitably shaped envelope allowing better control of the strength of the plasma and the duty cycle would be preferable.

### Discussion

The results reported above provide information on the magnitude or relative magnitude of plasma-induced velocities, their penetration into the surrounding air and frequency response of the air to the unsteady electrodynamic forcing. The purpose of this discussion is to assess this information with regard to the requirements for turbulent boundary layer drag reduction using an oscillating wall as discussed in the introduction .

The references on oscillating wall drag reduction<sup>11-19</sup> indicate that drag reduction occurs when the non-dimensional frequency is around 0.01 and the peak non-dimensional wall displacement is greater than the

spanwise low speed streak correlation length. For estimating the plasma induced motion requirements for a low speed wind tunnel test at 10 m/s, it is assumed that  $F^+ = Fv/u_\tau^2 = 0.01$  and  $\Delta X^+ = \Delta X u_\tau/v = 100$  are representative values where a measurable effect would be expected. Assuming a sinusoidal oscillation and standard ambient conditions of 760mmHg and 20 deg C, these data correspond to a plasma-induced motion requirement of  $F = 137\text{Hz}$  and  $U_x = 2.8\text{ m/s}$  where  $U_x$  is the peak spanwise velocity.

If the absolute peak velocity in Figure 11 corresponding to 0 dB is assumed to be 1.6 m/s (from Figure 9), the data are already below the target velocity of 2.8 m/s by about a factor of two. While this could probably be corrected by optimizing the electrode design and increasing the excitation amplitude, the data further roll-off at a high rate. At the 137 Hz target frequency, there was no measurable oscillation signal above the noise level. It is clear, therefore, that the target conditions for the proposed low-speed drag-reduction test are not likely to be attained with the current method.

Aside from the oscillatory aspects of the problem, there are other physical considerations. As opposed to the oscillating wall, which is a smooth translation over a wide area, the strip electrodes are inherently three-dimensional. It was shown in the first plasma flow control test at Langley<sup>1,2</sup>, that streamwise oriented plasma electrodes generate unstable vortices with steady state excitation due to the bilateral mean flow. In addition, even if the plasma duty cycle problem discussed earlier were corrected, as the oscillation frequency increases, a behavior similar

to the steady-state results would be expected. A further issue is that of scaling to flight conditions. If physics and the non-dimensional frequency requirement of  $F^+ = 0.01$  holds at flight conditions, an unlikely situation, the required frequency would be in excess of 1 MHz. Even if the scaling did not hold, a frequency very much higher than the current target of 137 Hz for a 10 m/s low speed test would be expected. Overall, the lack of adequate amplitude and frequency response along with the three dimensionality of the plasma electrodes and mean flow effects indicate that the proposed approach will probably not work as an alternative to the mechanically oscillated wall.

There is no indication of any significant scalability in the method that would allow use at the high Reynolds numbers and high subsonic Mach numbers required for flight. While the body force strength can be increased by increasing the amplitude of the excitation voltage, the breakdown strength of the dielectric becomes the limiting parameter. The materials used in these experiments were already selected based on their high breakdown voltage and further gains in this area using currently available materials would most likely be incremental. Higher excitation frequencies required in flight also exacerbate the material robustness issue. In developing the models for the current experiments doubling the excitation frequency to 6 kHz caused a large increase in the model failure (burn-through) rate. Operation at 10 kHz could only be done on an intermittent basis without igniting the plastic model.

The excursion into the phase-averaged ICCD photographs was actually a

precursor to planned use of the camera for particle flow visualization. That activity has not yet been started but the camera proved to be very useful in capturing the structure of the plasma as seen in Figures 6 and 8. Since the plasma body force is associated with the steep electric field gradient at the instantaneous cathode of a normal glow discharge, only the cathode picture in Figure 8 may be responsible for the gas motion. While there are two plasma pulses per excitation cycle (Figure 13(b)), only one seems to be responsible for the observed flow behavior. That raises the question as to what the anode pulse does to the flow or to the system efficiency.

Another issue raised by the Figure 6 and 8 photographs has to do with theoretical and computational modeling. Clearly, one would prefer not to have to deal with the spatial and temporal randomness and complexity of the observed plasma patterns in order to compute the plasma body force. The simplified force model used in reference 3 indicates that this is possible for steady state applications. A simplified dynamic force model is also required.

#### **Summary and Conclusions**

This study was an attempt to develop a plasma-based analog to a mechanically oscillated wall. The guiding consideration was that the lateral oscillations were the operative feature in controlling turbulence production, and that the oscillations could be achieved in various ways, such as, with a plasma-induced flow. The current concept was not carried through to wind tunnel drag measurements because bench testing showed problems with the approach. The main finding was that the plasma-

induced oscillations rolled off rapidly with frequency and were not able to meet the requirements for a low speed test. Also, the oscillations were accompanied by a bi-lateral mean flow along the electrodes. Such motion is characteristic of steady-state excitation and has been shown to cause streamwise vortex formation. The prognoses, therefore, for this particular plasma drag reduction approach is not favorable.

The study, however, produced noteworthy findings with respect to the plasma itself and experimental techniques. Phase-averaged, 10  $\mu$ sec duration photographs show distinctly different, very non-uniform light patterns for the instantaneous anode and cathode. This could have implications for flow modeling studies.

A successful model design and excitation method were developed with the triad electrode actuators driven by a quadrature output power supply. With respect to diagnostics, the hot-wire anemometer was shown to be a useful tool for studying the plasma-induced flow provided the entire unit is electrically isolated. Even with isolation, however, polarization discharge or glow discharge from the probes can cause significant measurement errors.

In conclusion, the lack of success for current study should not reflect unfavorably on the study of flow control with plasma-induced motions in general. A number of studies are currently underway and no doubt more are planned. What the current study shows is that applications should be sought on scale in keeping with the plasma-induced body force strength limitations. Instead of trying to oscillate the entire

wall region of the boundary layer, for example, a more focused approach targeting local turbulent motions close to the wall could be studied.

### References

1. Roth, J.R., Sherman, D.M. and Wilkinson, S.P., Boundary layer flow control with a one atmosphere uniform glow discharge surface plasma, AIAA paper 98-0328, 1998.
2. Roth, J.R., Sherman, D.M., and Wilkinson, S.P., Electrohydrodynamic flow control with a glow-discharge surface plasma. AIAA Journal. 38(7), July 2000, pp. 1166-1172.
3. Corke, T.C., Jumper, E.J. Post, M.L., McLaughlin, T.E., Application of weakly-ionized plasma as wing flow control devices, AIAA paper 2002-0350, 2002
4. Lorber, P., McCormick, T., Anderson, T., et al., Rotorcraft Retreating Blade Stall Control, AIAA paper A00-33875, 2000.
5. Roth, J.R., Method and apparatus for covering bodies with a uniform glow discharge plasma and applications thereof. US Patent 5,669,583, Sept. 23, 1997.
6. Sherman, D.M., S.P. Wilkinson, and J.R. Roth, Paraelectric Gas Flow Accelerator. US Patent US 6200539 B1, March 13, 2001
7. Roth, J.R., Industrial Plasma Engineering, Volume 2, Applications to Nonthermal Plasma Processing. Vol. 2., Institute of Physics Publishing, 2001
8. Roth, J.R., Industrial Plasma Engineering, Volume 1, Principles. Vol. 1, Institute of Physics Publishing 1995, pp. 453-461.
9. Massines, F., Rabehi, A. Decomps, P., Gadri, R.B., et al., Experimental and theoretical study of a glow discharge at atmospheric pressure controlled by a dielectric barrier, Journal of Applied Physics. 83(6), March 15, 1998, pp. 2950-2957.
10. Kunhardt, E.E., Generation of large-volume, atmospheric-pressure nonequilibrium plasmas. IEEE Transactions on Instrumentation and Measurements. 28(1), February, 2000 pp.189-200.
11. Akhavan, R., W. Jung, and N. Mangiavacchi, Control of wall turbulence by high frequency spanwise oscillations, AIAA Paper 93-3282, 1993.
12. Choi, J.-I., C.-X. Xu, and J.H. Sung, Drag reduction by spanwise wall oscillations in wall-bounded turbulent flows, AIAA Journal, 40(5), May, 2002 pp.842-850.
13. Trujillo, S.M., D.G. Bogard, and K.S. Ball, Turbulent boundary layer drag reduction using an oscillating wall, AIAA Paper 97-1870, 1997.
14. Artana, G., et al., Flow Control with Electrohydrodynamic Actuators, AIAA Paper A01-16253, 2001
15. Dhanak, M.R. and C. Si, On reduction of turbulent wall friction through spanwise wall oscillations. Journal of Fluid Mechanics. Vol. 383, 1999, pp. 175-195.

16. Baron, A. and M. Quadrio, Turbulent drag reduction by spanwise wall oscillations. Applied Scientific Research, Vol. 55, 1996, pp. 311-326.
17. Choi, K.-S. and M. Graham, Drag reduction of turbulent pipe flows by a circular-wall oscillation. Physics of Fluids. 10(1), January, 1998 pp. 7-9.
18. Choi, K.-S., Roach, P.E. DeBisschop, J.-R., Clayton, B.R., Turbulent boundary-layer control by means of spanwise-wall oscillations, AIAA paper 97-1795. 1997.
19. Laadhari, F., L. Skandaji, and R. Morel, Turbulence reduction in a boundary layer by a local spanwise oscillating surface. Physics of Fluids. 6(10), October, 1994, pp.3218-3220.
20. Gadri, R.B., One Atmosphere Glow Discharge Structure Revealed by Computer Modeling. IEEE Transactions on Plasma Science. 27(1), February, 1999 p.1999 36-37
21. Kidron, I., Measurements of the transfer function of hot-wire and hot-film turbulence transducers, IEEE Transactions on Instrumentation and Measurements, IM-15(3), September 3, 1966, pp.76-81.

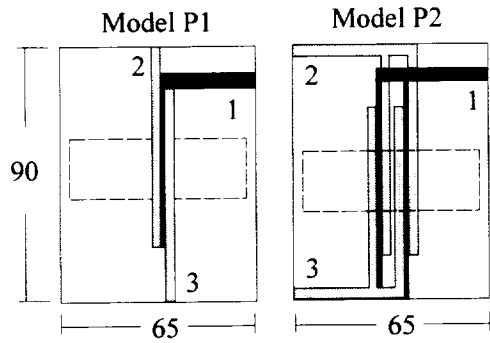


Figure 1. Plasma test models. Dashed rectangle represents test area. Numbers are terminal designations. Black traces top surface, gray traces bottom surface. Units millimeters.

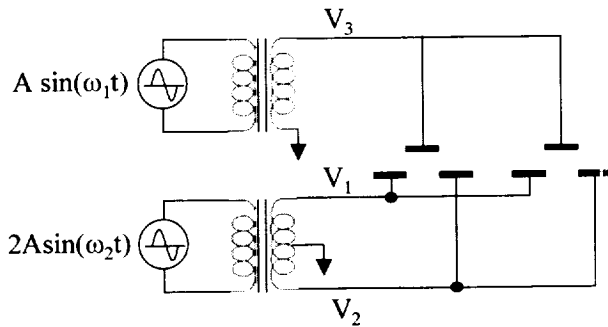


Figure 2. Plasma power supply and model hook-up. Bars represent top and bottom surface electrodes. (Dielectric not shown.)

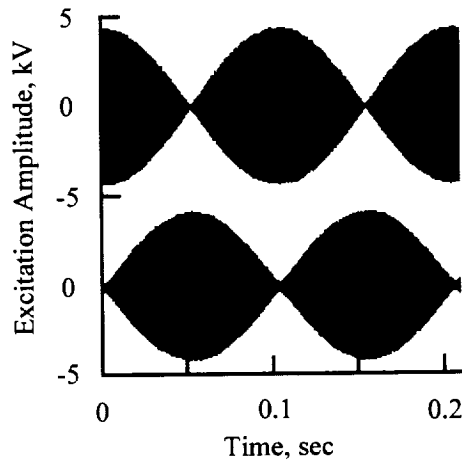


Figure 3. Example of differential excitation voltage across dielectric. In Figure 2, these represent  $V_1-V_3$  and  $V_2-V_3$

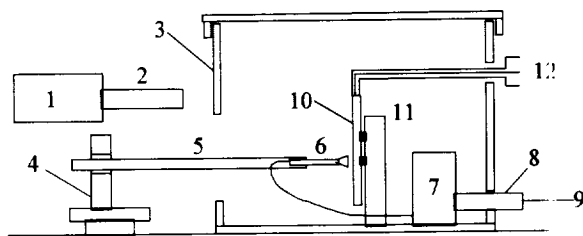


Figure 4. Experimental bench setup. (1) ICCD camera, (2) lens, (3) clear plastic box enclosure, (4) 3-axis probe survey mechanism, (5) non-conducting probe extension arm, (6) hot-wire probe, (7) anemometer, (8) optical isolator, (9) cable to data acquisition system, (10) plasma model, (11) model support, (12) plasma power leads

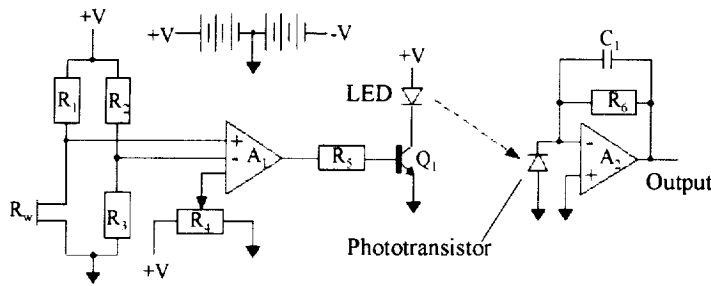


Figure 5. Schematic of hot-wire anemometer and optical isolator.

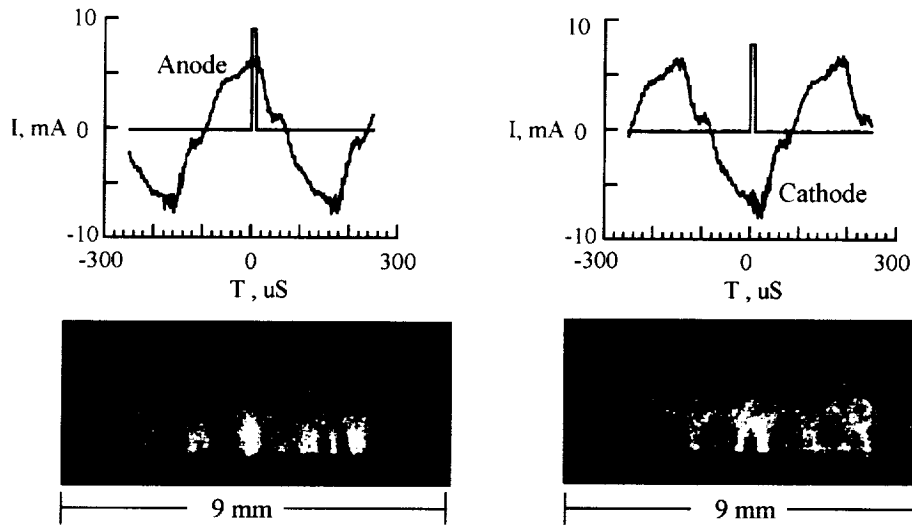


Figure 6. ICCD phase-averaged photographs of plasma along edge of electrode. Plots show camera trigger with respect to plasma current. Camera exposure: 10  $\mu$ sec per shot, 20 shots per photograph. Excitation:  $\sim 8.5$  kVp-p at 3 kHz.

Figure 7. Hot wire wall proximity effect in still air. Overheat ratio  $R_{hot}/R_{cold}=1.5$ ,  $R_{cold} \sim 3.5 \Omega$ ,  $5 \mu\text{m}$  diameter platinum-plated Tungsten. Wall and wire axis vertical. Prongs normal to wall.

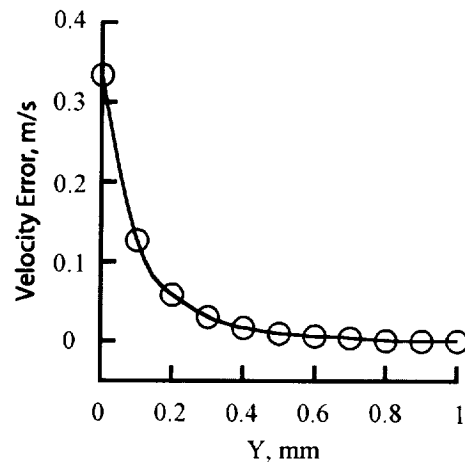


Figure 8. ICCD camera phase-averaged photographs of pitot probe tip at various electrical potentials. Excitation voltage  $\sim 8.5\text{kVp-p}$ , 3kHz. Exposure: 10  $\mu\text{sec}$  pr shot, 20 shots per photograph.

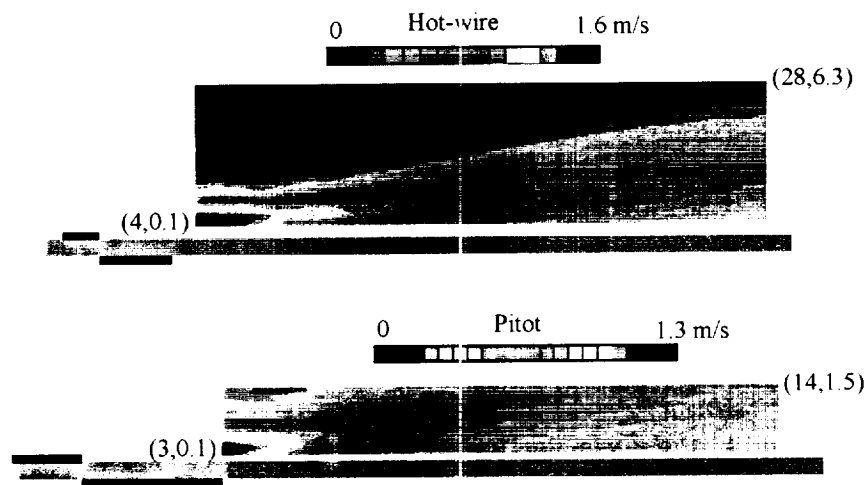
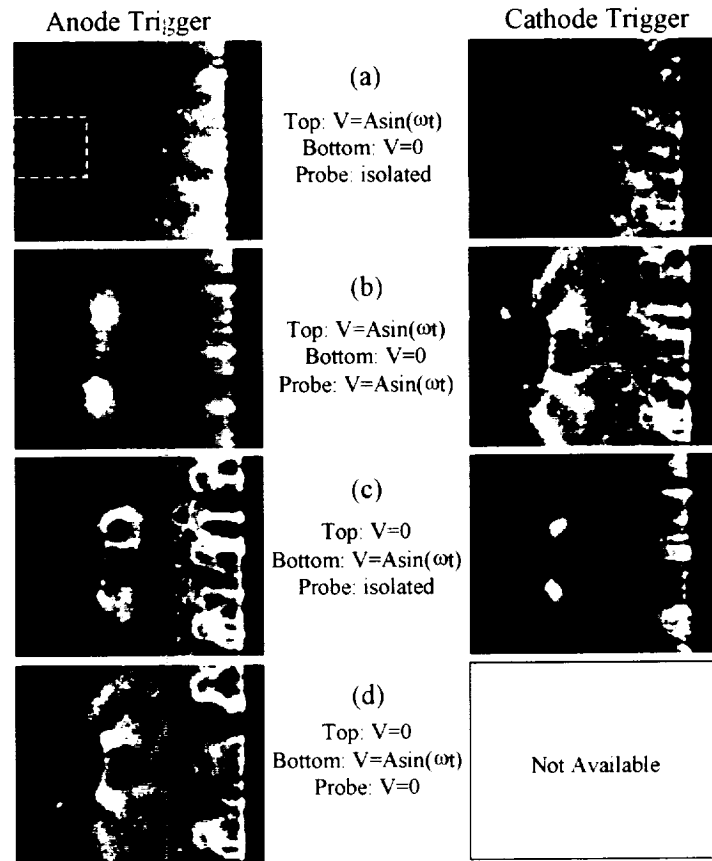


Figure 9. Contour maps (color) of mean velocity magnitudes from hot-wire and pitot probes. Bracketed numbers are (X,Y) coordinates of corners of contour maps in millimeters. Y=0, top surface; X=0, right edge of top electrode. Scale and color legend different for each map. Excitation is single-phase 8.47kV p-p at 3 kHz.

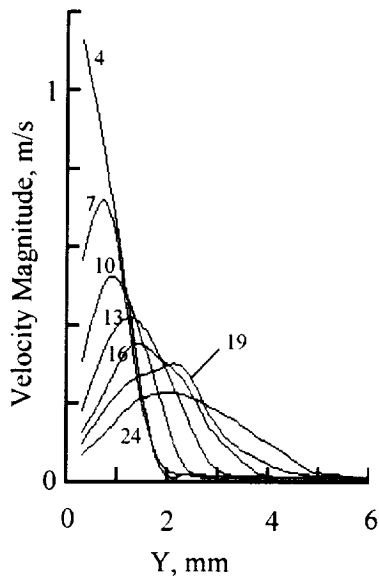


Figure 10. Velocity magnitude profiles at various X locations (denoted by labels in mm)

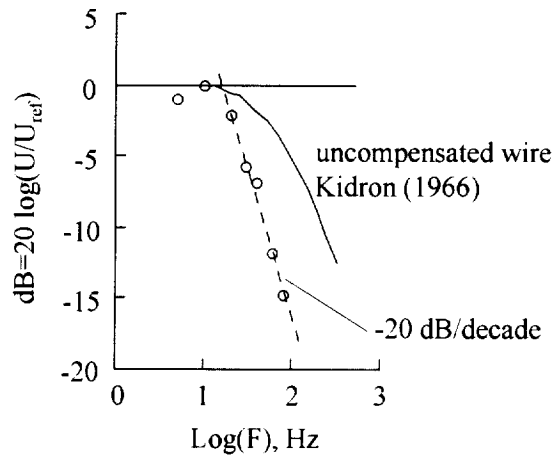


Figure 11. System frequency response measured with hot wire (symbols)

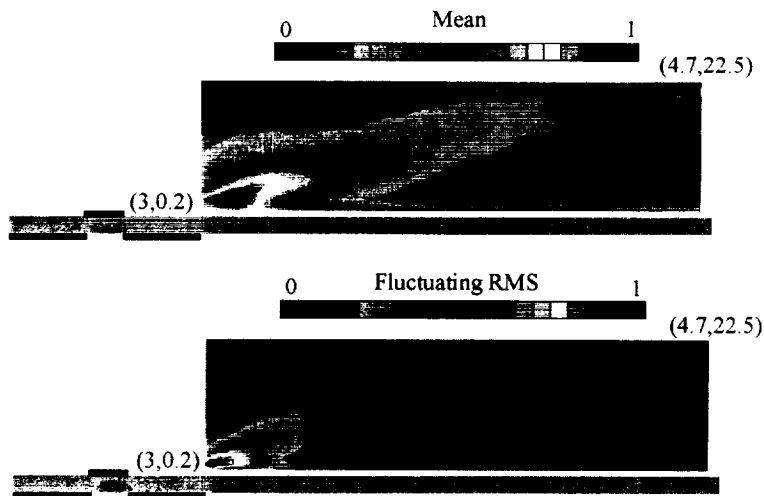


Figure 12(a) and 12(b). Contour plots (color) of mean and fluctuating velocity magnitude for Model P1  $F=20$  Hz. Excitation is two-phase 8.76 kV p-p at  $\omega_1=3000$  and  $\omega_2=3020$  kHz. Map corner coordinates (X,Y) shown in parentheses. Color legends apply to individual maps only.

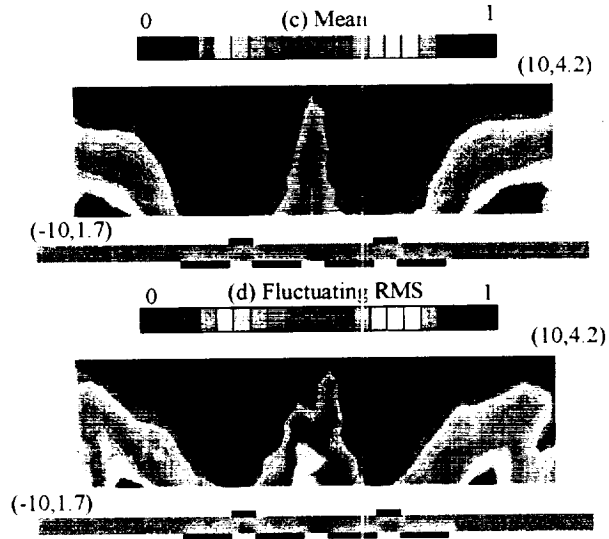


Figure 12(c) and 12(d). Contour plots (color) of mean and fluctuating rms velocity magnitude for Model P2. Excitation is 8.76 kV p-p at  $\omega_1=3000$  and  $\omega_2=3020$  kHz. Map corner coordinates (X,Y) are shown in parentheses. Color legends apply to individual maps only.

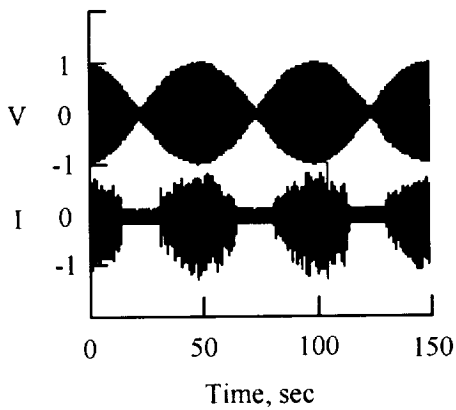


Figure 13(a). Typical voltage and current excitation waveforms ( $V_1-V_3$  or  $V_2-V_3$ ) (peak normalized).

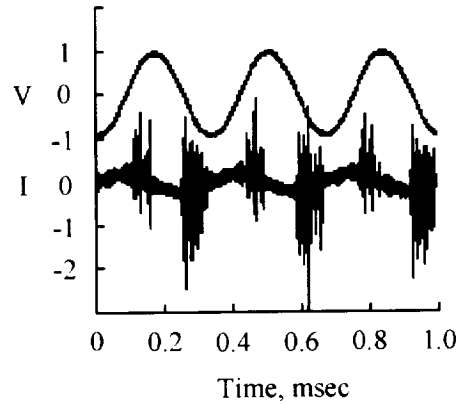


Figure 13(b). Expanded one millisecond time interval of an envelope peak in 13(a).

